THE JOURNAL OF BIOLOGICAL CHEMISTRY VOL. 291, NO. 35, pp. 18239–18251, August 26, 2016

Hook Adaptors Induce Unidirectional Processive Motility by Enhancing the Dynein-Dynactin Interaction*

Received for publication, May 16, 2016, and in revised form, June 30, 2016 Published, JBC Papers in Press, June 30, 2016, DOI 10.1074/jbc.M116.738211

Mara A. Olenick[‡§], Mariko Tokito[‡], Malgorzata Boczkowska[‡], Roberto Dominguez[‡§], and Erika L. F. Holzbaur[‡§1]

From the [‡]Department of Physiology and Pennsylvania Muscle Institute and [§]Biochemistry and Molecular Biophysics Graduate Group, Perelman School of Medicine at the University of Pennsylvania, Philadelphia, Pennsylvania 19104

Cytoplasmic dynein drives the majority of minus end-directed vesicular and organelle motility in the cell. However, it remains unclear how dynein is spatially and temporally regulated given the variety of cargo that must be properly localized to maintain cellular function. Recent work has suggested that adaptor proteins provide a mechanism for cargo-specific regulation of motors. Of particular interest, studies in fungal systems have implicated Hook proteins in the regulation of microtubule motors. Here we investigate the role of mammalian Hook proteins, Hook1 and Hook3, as potential motor adaptors. We used optogenetic approaches to specifically recruit Hook proteins to organelles and observed rapid transport of peroxisomes to the perinuclear region of the cell. This rapid and efficient translocation of peroxisomes to microtubule minus ends indicates that mammalian Hook proteins activate dynein rather than kinesin motors. Biochemical studies indicate that Hook proteins interact with both dynein and dynactin, stabilizing the formation of a supramolecular complex. Complex formation requires the N-terminal domain of Hook proteins, which resembles the calponin-homology domain of end-binding (EB) proteins but cannot bind directly to microtubules. Single-molecule motility assays using total internal reflection fluorescence microscopy indicate that both Hook1 and Hook3 effectively activate cytoplasmic dynein, inducing longer run lengths and higher velocities than the previously characterized dynein activator bicaudal D2 (BICD2). Together, these results suggest that dynein adaptors can differentially regulate dynein to allow for organelle-specific tuning of the motor for precise intracellular trafficking.

Microtubules provide a polarized highway to facilitate the transport of organelles and vesicles throughout the cell. The minus ends of microtubules are usually nucleated near the cell center, with the plus ends oriented outward, toward the cell periphery. This polarity ensures that microtubule motors drive motility in a specific direction; kinesin motors generally drive plus end motility, whereas minus end traffic is primarily driven by cytoplasmic dynein. Regulation of these opposing motors is vital for cell survival, particularly in specialized cells like neurons that require efficient transport over long distances (1). However, it remains unclear how microtubule motors are spatially and temporally regulated to control the intracellular trafficking of specific cargo. As a single major form of cytoplasmic dynein drives the transport of a wide array of cargos, including endosomes, RNA granules, and mitochondria (2–4), it is likely that the transport properties of dynein are modulated by the binding of cargo-specific adaptor molecules.

A number of dynein regulatory and adaptor proteins have been identified to date, including dynactin, Lis1, bicaudal D2 (BICD2)[2], and, more recently, Hook proteins. The first major regulator to be identified was dynactin, a large multisubunit protein complex required for most functions of dynein within the cell. Dynactin forms a co-complex with dynein (5–8) that enhances the initial recruitment of dynein to the microtubule (9, 10) and mediates the association of dynein with some intracellular cargos (11–14). A second major dynein regulator, Lis1, binds to the dynein motor domain and blocks the required linker swing in the mechanochemical cycle for dynein; thus, Lis1 binding induces a non-motile state of dynein that binds tightly to the microtubule (15). In contrast to the inhibitory effect of Lis1 on dynein motility, the dynein adaptor BICD2 has been shown to induce superprocessive motility of dynein, potentially through enhanced stability of the dynein-dynactin complex (16, 17). Yet another mechanism adaptors can use to regulate transport is coordination of different motors on the same cargo. For instance, JIP1 acts as a switch between dynein- and kinesin-1-mediated transport, depending on its phosphorylation state (18). Given the wide variety of cargo that must be properly localized within eukaryotic cells, it is likely that many additional adaptors and their underlying regulatory mechanisms remain to be identified and characterized.

Here we focus on another family of potential dynein adaptors, Hook proteins. Genetic screens in fungal model systems have provided evidence that Hook proteins are required for early endosome trafficking. In general, Hook proteins are characterized by three conserved regions: a globular N-terminal putative microtubule binding domain, a central coiled-coil domain, and a variable and predicted unstructured C-terminal

* This work was supported by National Institutes of Health Grants P01 GM087253 (to E. L. F. H. and R. D.) and T32 GM07229 (to M. A. O.). The authors declare that they have no conflicts of interest with the contents of this article. The content is solely the responsibility of the authors and does not necessarily represent the official views of the National Institutes of Health.

[1] To whom correspondence should be addressed: Dept. of Physiology, Perelman School of Medicine at University of Pennsylvania, 630 Clinical Research Bldg., 415 Curie Blvd., Philadelphia, PA 19104. Tel.: 215-573-3257; E-mail: holzbaur@mail.med.upenn.edu.

[2] The abbreviations used are: BICD, bicaudal D; EB, end-binding; CAP, cytoskeleton-associated protein; FTS, Fused Toes; FHIP, Fused Toes and Hook-interacting protein; Htag, Halo tag; TMP, trimethoprim; DHFR, dihydrofolate reductase; MTOC, microtubule organization center; DIC, dynein intermediate chain; IP, immunoprecipitation; GMPCPP, guanosine-5′-[(α,β)-methyleno]triphosphate; aa, amino acids; TIRF, total internal reflection fluorescence; MT, microtubule.

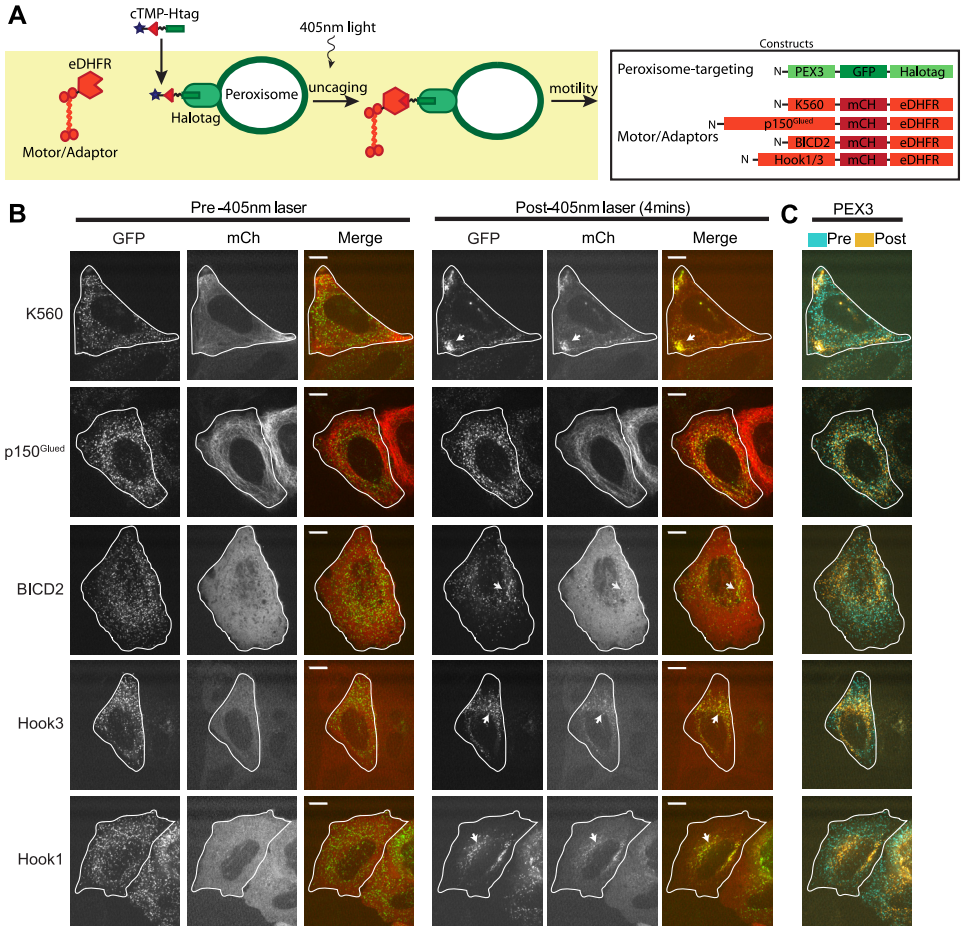

FIGURE 1. **Hook proteins redistribute peroxisomes to the perinuclear region in an optogenetic assay.** *A*, schematic of inducible the dimerization assay and corresponding constructs. *B*, using a photoactivatable dimerization system (cTMP-Htag dimerizer) (48), motors/adaptors (-mCh-DHFR tagged) were recruited to peroxisomes (PEX3-Halo-GFP-labeled) by 405-nm light, and the resulting motility was observed by live cell confocal microscopy. *Scale bars* = 10 μm. *Arrows* indicate peroxisome clustering after recruitment. *C*, overlay of pre- and post-dimerization images of peroxisomes.

domain thought to mediate cargo binding (19). In *Aspergillus nidulans*, HookA was described as an adaptor on early endosomes regulating dynein, whereas Hok1 in *Ustilago maydis* was shown to coordinate dynein and kinesin-3 motors during early endosome transport (20, 21). In both fungal Hook proteins, the C terminus attaches to cargo through interaction with the proteins Fused Toes (FTS) and FTS and Hook-interacting protein (FHIP) (20–22).

These studies led us to ask whether such functions of Hook proteins were conserved in mammalian systems. There are three Hook isoforms expressed in humans: Hook1, Hook2, and Hook3. Each isoform has been associated with a different cargo. Hook3 localizes to the Golgi (19), Hook2 is recruited to centrosomes (23), and Hook1 is implicated in endosomal transport (24–26). To explore adaptors with roles in cargo transport, we focused on Hook1 and Hook3 in our studies.

We used complementary optogenetic and single-molecule approaches to establish mammalian Hook proteins as motor adaptors enhancing unidirectional minus end-directed motility driven by dynein. We show that both Hook1 and Hook3 enhance the formation of a dynein-dynactin complex. The formation of this complex requires the N-terminal globular domain of Hook proteins. Contrary to previous suggestions, this domain does not bind to microtubules directly. In single-molecule assays, we find that both Hook1 and Hook3 induce highly processive dynein motility, resulting in both longer run lengths and faster velocities than the previously characterized dynein activator BICD2. Together, these results support a model in which organelle-specific adaptors differentially regulate dynein motor function within the cell.

Results

Differential Regulation of Dynein-mediated Cargo Transport by Hook Proteins—To assess the role of different adaptors in cargo transport within the cell, we used a light-induced dimerization system to observe changes in cargo motility after recruitment of different adaptors and regulators. In this system, we use the dimerizer cTMP-Htag, a small molecule made of a Halo tag (Htag) ligand linked to a photocaged trimethoprim (TMP). This molecule heterodimerizes HaloTag proteins (Halo) and *Escherichia coli* DHFR (eDHFR)-tagged proteins. In our experiments, dimerization between a Halo-tagged cargo and a DHFR-tagged adaptor/motor is induced using 405-nm light to cleave photocaged cTMP-Htag (27) (Fig. 1*A*). We used peroxisomes as a model organelle because they are not very motile under endogenous conditions and are uniformly distributed throughout the cell (28), making them ideal to observe changes in motility.

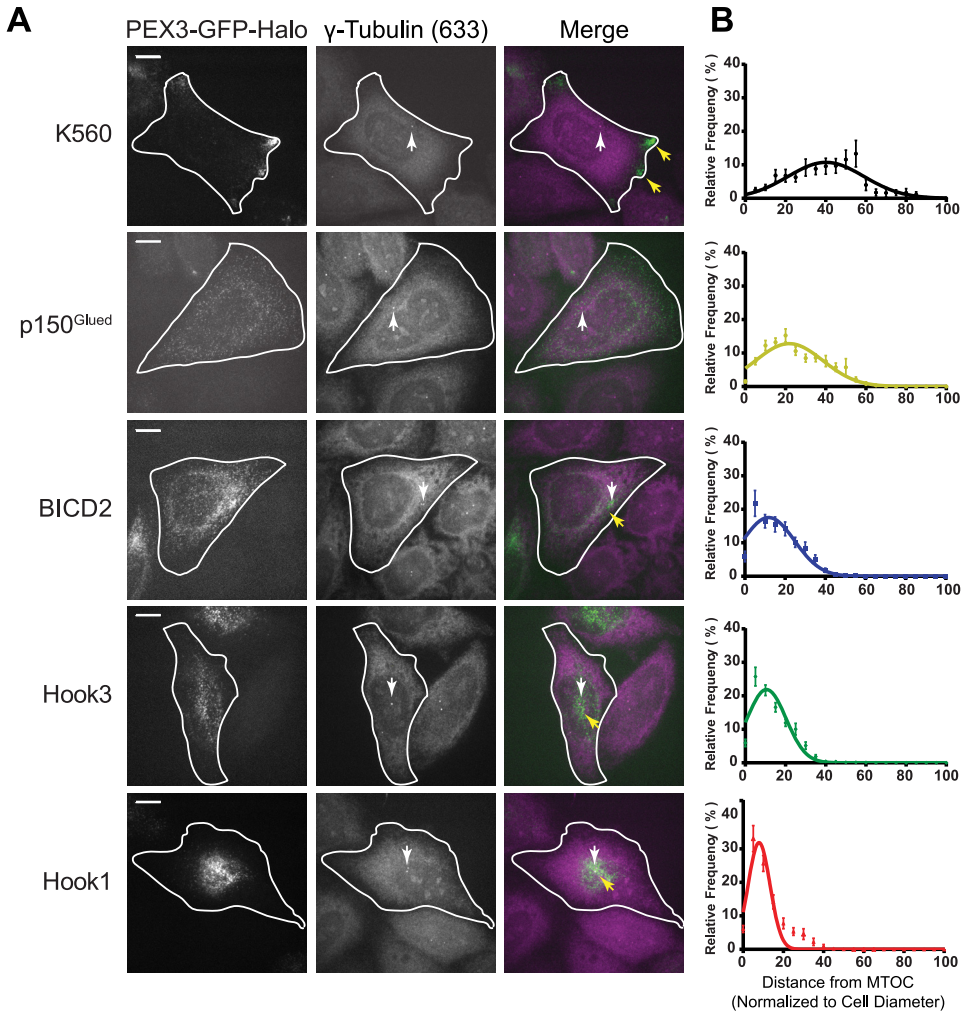

FIGURE 2. **Hook proteins differentially redistribute peroxisomes to the MTOC.** *A*, dimerization assay in fixed cells stained with γ-tubulin antibody. Images are maximum projections of confocal z stacks. *Scale bars* = 10 μm. *White arrows* point to γ-tubulin stained MTOC, and *yellow arrows* point to peroxisome clusters. Cell outlines were determined from corresponding X-mCH-DHFR images (data not shown). *B*, distribution of peroxisomes from MTOC measured in a fixed time point dimerization assay (analyzed using Cell Profiler (47)). The endosomally linked adaptor Hook1 tightly clusters peroxisomes to the MTOC compared with Hook3 and BICD2. Cells analyzed per condition: K560, $n = 36$; p150^{Glued}, $n = 19$; BICD2, $n = 26$; Hk1, $n = 23$; Hk3, $n = 32$. *Error bars* show standard error based on number of cells.

In live cell experiments in HeLa cells, recruitment of either Hook1 or Hook3 to peroxisomes through light-induced dimerization resulted in a pronounced redistribution of peroxisomes toward the perinuclear region (Fig. 1, *B* and *C*). The organelle redistribution induced by either of the Hook proteins was similar to that observed upon recruitment of the known dynein activator BICD2, suggesting that Hook proteins also act as dynein adaptors (Fig. 1, *B* and *C*). In contrast, recruitment of the dynein-binding protein p150^{Glued} was not sufficient to induce robust global redistribution of peroxisomes in this assay. We used K560 (a constitutively active construct of kinesin-1) as a control for kinesin motility and observed robust motility to the periphery of the cells (Fig. 1, *B* and *C*). For additional controls, we also imaged cells expressing these constructs in the absence of dimerizer or in the absence of photobleaching and saw no effects on peroxisome location or motility (data not shown).

To quantify the redistribution phenotype of each adaptor, we measured the distance of each peroxisome from the microtubule organization center (MTOC) in cells that were fixed 45 min after addition of an uncaged TMP-Htag dimerizer and then stained with a γ-tubulin antibody to visualize the MTOC. Analysis of cells from three independent repeats showed that Hook1, Hook3, and BICD2 each induced a pronounced concentration of peroxisomes near the MTOC in contrast to either p150^{Glued} or K560 (Fig. 2). Direct comparison of the distributions shows that Hook1 induced the tightest clustering of peroxisomes near the MTOC, whereas recruitment of either Hook3 or BICD2 induced similar distributions (Fig. 2). Of note, both Hook3 and BICD2 have been linked to Golgi transport (19, 29), whereas Hook1 has been linked to endosomal transport (24). Although p150^{Glued} was efficiently recruited to peroxisomes in this assay (Fig. 2), this recruitment was not sufficient to induce marked peroxisome motility or redistribution, consistent with the idea that dynactin alone is insufficient to induce superprocessive motility. Together, these observations suggest that, like BICD2, both Hook1 and Hook3 can activate dynein motility and that differences among these activators may tune dynein activity to regulate cargo-specific transport.

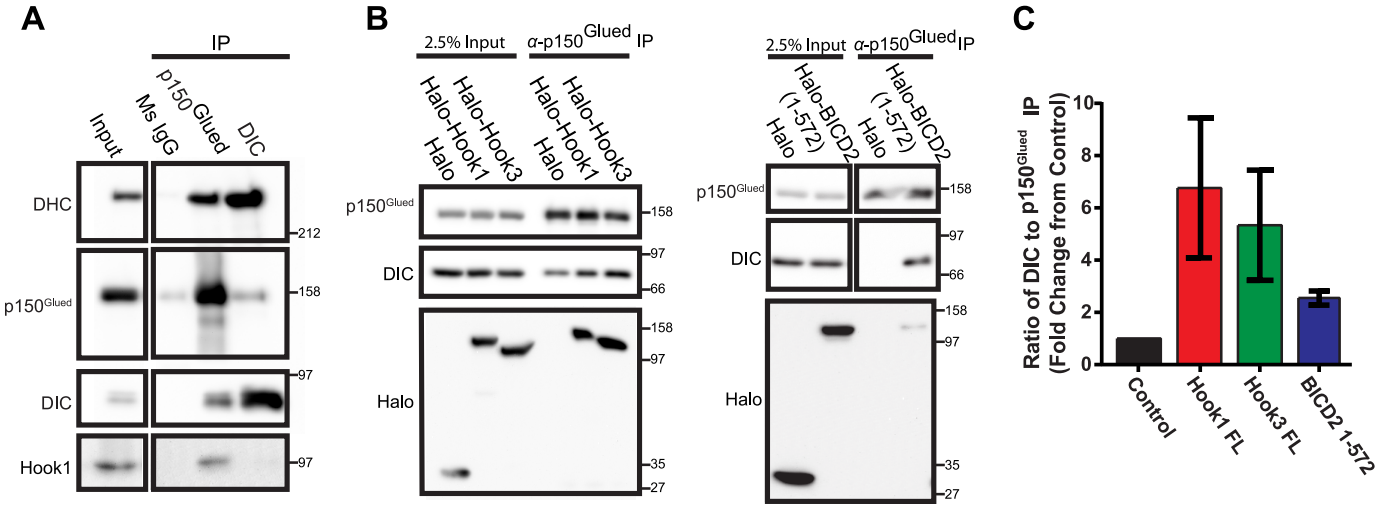

FIGURE 3. **Mammalian Hook proteins interact with the dynein-dynactin complex.** *A*, Western blot showing IP of endogenous p150^{Glued} (subunit of dynactin) and DIC from mouse brain lysates, with anti-myc used as a mouse IgG (*Ms IgG*) control. IP of p150^{Glued} shows interaction with Hook1, whereas disruption of the dynein-dynactin complex in IP with anti-DIC shows loss of this interaction ($n = 3$). *B*, Western blots showing IP of endogenous p150^{Glued} from COS7 cells expressing Halo-Hook1, Halo-Hook3, and Halo-BICD2 (1–572), with the HaloTag expressed as a negative control. *C*, graph of the DIC- to-p150^{Glued} IP ratio from the experiments in *B* ($n = 4$). The ratio of DIC to p150^{Glued} IP for the control condition (HaloTag only) was normalized to 1, and all other conditions are shown as a -fold change from the control. *Error bars* show standard error.

Mammalian Hook Proteins Interact with Dynein-Dynactin—To characterize the interactions of mammalian Hook proteins with dynein and dynactin, we performed immunoprecipitation experiments using endogenous and expressed Hook proteins. Using mouse brain lysates, we immunoprecipitated endogenous dynein and dynactin with monoclonal antibodies to the dynein intermediate chain (DIC) and the p150^{Glued} subunit of dynactin, respectively. Co-immunoprecipitation of endogenous Hook1 was seen with the anti-p150^{Glued} antibody but not with the anti-DIC antibody (Fig. 3*A*). This DIC antibody is known to disrupt the interaction of dynein with dynactin (5), as confirmed by a decreased amount of p150^{Glued} in the DIC IP lane (Fig. 3*A*). These results suggest that Hook proteins either interact with dynactin directly or with the full dynein-dynactin complex rather than solely with dynein.

Next we performed IP experiments using Halo-tagged Hook proteins expressed in COS7 cells. Again using the p150^{Glued} antibody, we observed co-immunoprecipitation of expressed full-length human Hook1 and Hook3 with the dynein-dynactin complex. With the expression of Hook proteins, we also observed an increase in the co-precipitation of dynein by the anti-p150^{Glued} antibody compared with a control experiment in which only the Halo tag was expressed (Fig. 3*B*). We quantified the ratio of DIC:p150^{Glued} in the immunoprecipitates from each condition and observed that expression of Hook1, Hook3, or BICD2 each induced enhanced association of dynein with dynactin compared with control IPs (Fig. 3*C*). This observation is consistent with previous studies suggesting that BICD2 enhances dynein-dynactin complex stability (16, 30). Here we found that both Hook proteins were also able to enhance the stability of the dynein-dynactin complex.

The N-terminal Domain of Hook Proteins Does Not Bind Microtubules but Is Important for Interaction with the Dynein-Dynactin Complex—Because previous work suggested that the N-terminal globular domain of Hook proteins binds microtubules (19), we asked whether this domain was necessary for the motor adaptor function of Hook proteins. First, we assessed the ability of Hook proteins to bind microtubules in cell lysates. Using a HA-tagged Hook1 construct expressed in COS7 cells, we observed pelleting of HA-Hook1 with Taxol-stabilized microtubules (Fig. 4, *A* and *B*). However, because this assay utilized cell lysates, the apparent interaction of Hook1 with microtubules could be indirect. To test whether the N-terminal region of Hook proteins can bind microtubules directly, we purified recombinant proteins spanning the N-terminal domain of Hook1 for use in microtubule pelleting assays. We tested binding with Taxol- or GMPCPP-stabilized microtubules because they mimic different nucleotide states of microtubules and induce different tubulin conformations, which can affect binding of microtubule-associated proteins (31, 32). Purified Hook1 (1–443 aa) showed no observable pelleting with either Taxol- or GMPCPP-stabilized microtubules, suggesting that this protein has little or no affinity for microtubules (Fig. 4*C*). Next we tested a recombinant Hook3 N-terminal protein fused to a coiled-coil GCN4 leucine zipper to induce efficient dimerization. Again, we observed no co-pelleting of the purified protein with microtubules, in contrast to a construct of p150^{Glued} that binds to microtubules directly through its N-terminal CAP-Gly domain (33) (Fig. 4*C*).

Additionally, we used sequence analysis and structure prediction to compare the calponin homology domain at the N terminus of Hook isoforms with that of the well characterized microtubule-binding proteins EB1 and EB3. Although the overall calponin homology fold is well conserved in Hook proteins, the specific regions implicated in microtubule binding, according to an EM reconstruction of EB3 on microtubules (34), are very different in Hook proteins compared with EBs (Fig. 5, *A* and *B*). Additionally, EB1 residues implicated in microtubule association by mutagenesis studies, including His-18, Lys-66, and Leu-67 (35), are not conserved in Hook isoforms. In our alignment of Hook and EB sequences based on secondary structure conservation, the corresponding residues in Hook proteins

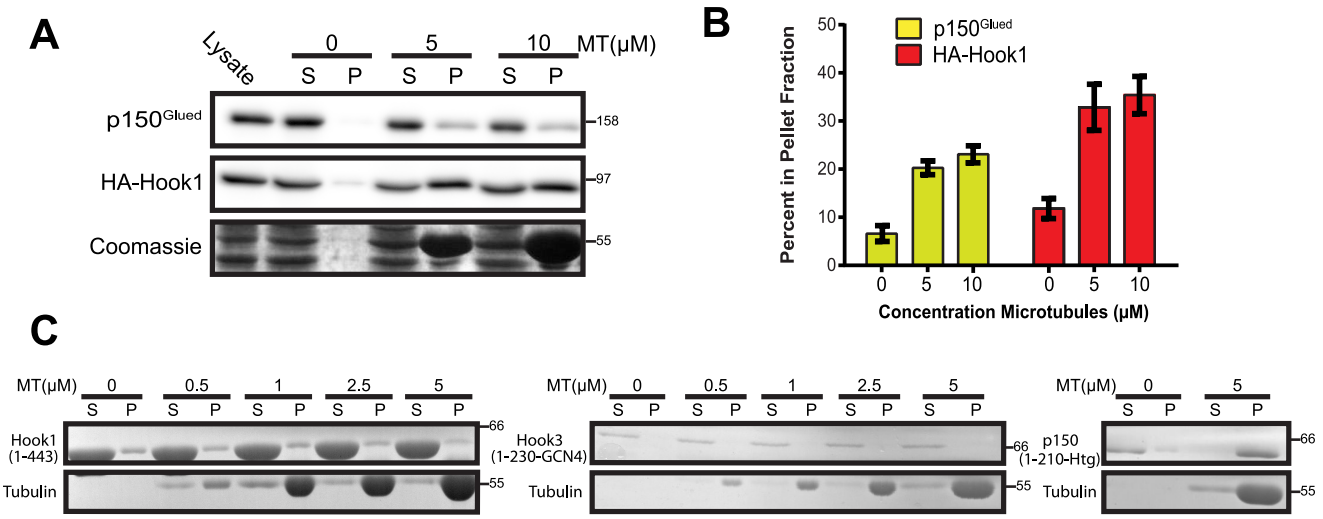

FIGURE 4. **Hook proteins bind microtubules indirectly.** *A* and *C*, MT binding assays were performed using cell lysates from HA-Hook1 transfected COS7 cells (*A*) and recombinant purified Hook1 dimer (1–443 aa) and Hook3 (1–210 aa-GCN4) (1 μM) (*C*). MT binding assays were performed by mixing equal amounts of protein to increasing amounts of Taxol- or GMPCPP-stabilized MTs. Supernatant (*S*) and pellets (*P*) were analyzed by SDS-PAGE gels and Western blotting, with the HA tag and p150^{Glued} antibodies as noted. The gels in *C* are Coomassie-stained SDS-PAGE gels. Hook1 from cell lysates co-sediments with MTs, but purified Hook1 and Hook3 constructs do not pellet with MTs, suggesting indirect binding. Endogenous and purified p150^{Glued} (1–210 aa-Htg construct) were used as controls. GMPCPP-stabilized MT binding assay gels are not shown. *B*, binding assay quantification of *A*. *Error bars* show standard error. Cell lysates experiments, $n = 5$; purified experiments, $n = 2–3$.

are the same or very similar to the mutations, H18E, K66E, and L67D, that cause a loss of microtubule binding in EB1, further suggesting that Hook proteins do not bind directly to microtubules. However, because we observed co-pelleting of Hook proteins expressed in cell lysates with microtubules, there is likely an indirect interaction mediated by the binding of Hook proteins to dynein-dynactin.

Structural studies of the dynein-dynactin-BICD2 complex indicate that a key aspect in the interaction is the extended coiled-coil domain of BICD2 that threads through a groove along the Arp1 filament (7, 8). Although there are similar extended coiled-coil domains in Hook proteins, the high sequence conservation of the N-terminal calponin homology domain among Hook isoforms made us question whether this region was also important for the interaction with dynein-dynactin. Using mouse brain lysates, we performed pulldown experiments with several Hook1 constructs, including the full-length protein, a construct lacking the N terminus (171–728 aa), and a construct truncated at the C terminus (1–554 aa) (Fig. 6*A*). COS7 cells expressing Halo-tagged Hook1 constructs were lysed and bound to Halo-link resin. Mouse brain lysates were then mixed with the resins as an abundant source of dynein-dynactin. The resulting pulldowns with full-length and C-terminally truncated Hook (1–554 aa) showed interaction with dynein and dynactin components, whereas the construct lacking the N-terminal region showed little or no interaction with dynein-dynactin (Fig. 6, *B* and *C*), consistent with work on other Hook homologs (20, 36). This result suggests that the N-terminal region of Hook proteins is necessary for the interaction with dynein-dynactin, potentially providing further contacts in addition to the coiled-coil region to modulate motor activity.

Hook Proteins Induce Highly Processive Runs with Enhanced Velocities—To characterize the functional effects of Hook adaptors on dynein, we utilized an *in vitro* single-molecule approach using total internal reflection fluorescence (TIRF) microscopy of cell extracts to characterize dynein-dynactin motility (10). We expressed Halo-tagged Hook constructs in HeLa cells and labeled cells with TMR-labeled HaloTag ligand prior to generation of cell lysates. We immobilized Taxol-stabilized microtubules to the coverslips of flow chambers using antibodies against β-tubulin. Cell lysates were diluted into motility buffer containing 10 mM magnesium ATP, Taxol, BSA, casein, and an oxygen-scavenging system and then flowed into the chamber to be imaged.

Using polarity-marked microtubules, Hook proteins were seen moving in a unidirectional manner to the minus ends of microtubules, as expected for dynein-mediated motility (Fig. 7*A*). The motility of Hook proteins could be inhibited using siRNA against the dynein heavy chain to knock down endogenous dynein, confirming that the motility seen is dynein-mediated (Fig. 7, *B* and *C*). Particles were tracked with Fiji TrackMate (37) to measure run lengths and velocity. The resulting data were analyzed with a custom maximum likelihood estimation modeling program in Matlab (38). Velocities were fit to single or double Gaussians as noted, and run lengths were fit to single exponential decay curves (Fig. 7, *D* and *E*).

Overall, full-length Hook1 and Hook3 proteins induced motility with higher velocities and longer run lengths compared with the active BICD2 construct 1–572 (Fig. 7*D*). More than 40% of the Hook-dependent motility events exhibited mean velocities of more than 1 μm/s (Fig. 7*F*) compared with a much lower percentage of high-velocity events observed with BICD2. Unlike the distribution of velocities observed for BICD2, which were adequately fit with a single Gaussian, the distributions for both Hook1 and Hook3 showed a distinct shoulder at higher velocities and were best fit to a double Gaussian function (Fig. 7*D*) (38). A similar complex distribution is evident in initial data on velocities of dynein-dynactin-Hook3 particles from McKenney *et al.* (16). We also noted that, within an individual run,

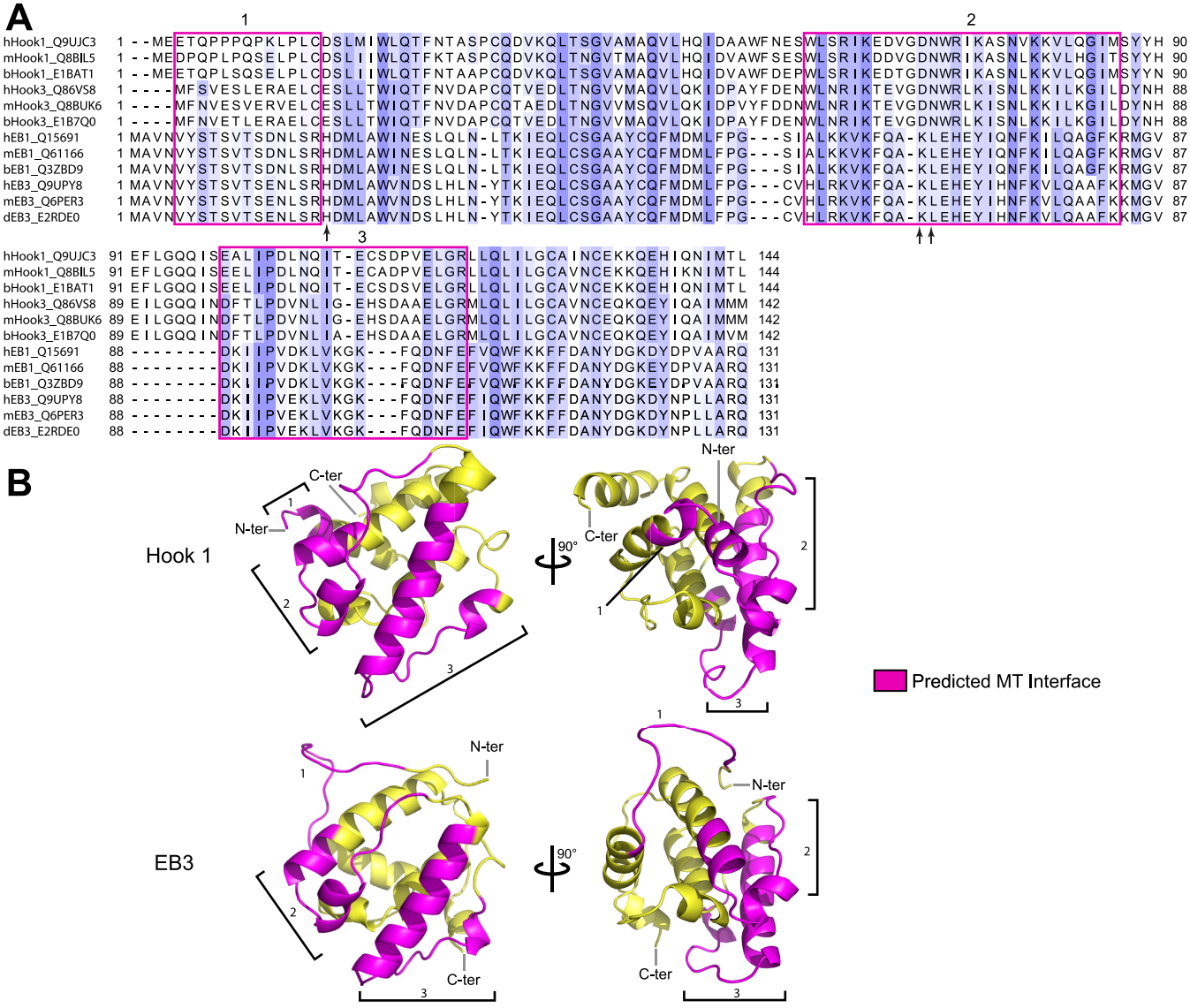

FIGURE 5. **Hook proteins lack conserved regions for MT binding.** *A*, sequence alignment based on the secondary structure for Hook1 and EB3. The coloring is based on the BLOSUM62 score. *Magenta boxes* indicate MT interaction regions in EB3 (residues within 6 Å of the tubulin surface in the PDB 3JAK structure (34)). *Arrows* indicate residues that ablate microtubule association in EB1 when mutated and are not conserved in Hook proteins (35). *B*, comparison of N-terminal mouse Hook1 (PDB code 1WIX) and EB3 (PDB code 3JAK (34)) structures with predicted microtubule interactions sites highlighted in *magenta*. Numbers correspond to *boxed regions* in the alignment (*A*). *C-ter*, C terminus; *N-ter*, N terminus.

Hook-positive particles showed more pronounced variations in instantaneous velocity than what was observed for BICD2-positive particles (Fig. 7*G*).

BICD2 is known to be autoinhibited, with truncation of the C terminus required for robust activation of dynein *in vitro* (16, 29, 39). In contrast, for both the optogenetic assay described above and these single-molecule approaches, full-length constructs of both Hook1 and Hook3 were active in our assay. However, we wondered whether truncating the C-terminal cargo-binding domain would result in further activation or perhaps reduce the variations in instantaneous velocities observed within runs of full-length Hook1 or Hook3. However, we found that truncated constructs of Hook1 and Hook3 lacking the C-terminal domains (Hook1 1–554 aa and Hook3 1–552 aa) moved at velocities very similar to those observed with the full-length proteins and displayed similar run lengths (Fig. 8*B*). Again, more than 40% of motility events exhibited mean velocities of more than 1 μm/s and displayed increased standard deviation in velocities within individual tracks, similar to the full-length proteins (Fig. 8, *C* and *D*). Thus, the observed variations in velocity during a single run are not likely to be due to transient folding of the Hook proteins into an autoinhibited conformation. We also tested several truncated coiled-coil constructs of Hook1 and Hook3, lacking both the N-terminal and C-terminal domains, but observed little to no motility with these constructs (Fig. 8*A*). Together, these observations suggest that the interaction of Hook proteins with dynein-dynactin is not solely mediated by the central coiled-coil regions but, instead, is likely to involve additional contacts with the N-terminal domain. Based on these observations, we suggest that an extended interaction interface involving both the N-terminal domain and the extended coiled-coil domains of Hook proteins

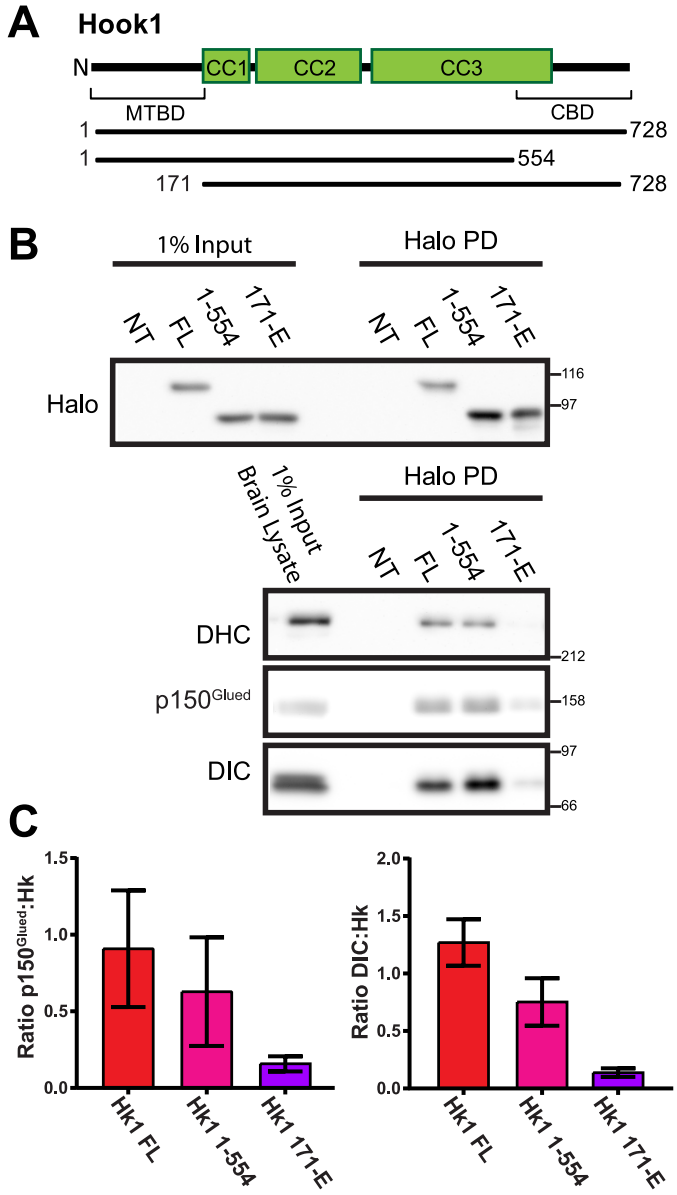

FIGURE 6. **Pulldown of Halo-Hook1 with the dynein-dynactin complex requires the N-terminal region.** *A*, conserved domains and predicted coiled-coil regions in Hook1. *MTBD*, putative microtubule binding domain; *CBD*, cargo binding domain. *B*, Western blot showing pulldown (*PD*) of Halo-Hook1 constructs with endogenous dynein-dynactin from mouse brain lysates. *DHC*, dynein heavy chain. Pulldown of the Hook1 full-length (*FL*) and Hook1 (1–554 aa) constructs shows interaction with dynein-dynactin, whereas pulldown of Hook1 (171–728 aa, *171-E*) shows loss of interaction with the dynein-dynactin complex. *NT*, non-transfected control. $n = 3$. *C*, graphs of DIC or p150^{Glued} to Hook1 (*Hk*) ratio from experiments in *B* ($n = 3$). *Error bars* show standard error.

may be necessary to induce the rapid velocities and longer run lengths we observed.

Discussion

Hook proteins have been implicated in the regulation of organelle transport in both fungal model systems and mammalian cells (20, 21, 24, 25). Here we used optogenetic and single-molecule approaches to examine the role of mammalian Hook proteins as motor adaptors. We found that mammalian Hook1 and Hook3 proteins enhance dynein-mediated motility. Although fungal Hok1 was suggested to function as a bidirectional adaptor (21), we did not find evidence that either Hook1 or Hook3 acts in this way. In our induced recruitment assay, targeting Hook proteins to peroxisomes induced rapid motility toward the perinuclear region, leading to organelle accumulation near the MTOC. These observations indicate activation of unidirectional, minus end-directed transport, which would not be expected for a bidirectional adaptor. However, it is possible that, in other systems, Hook proteins also promote kinesin-dependent motility. HeLa cells express 32 kinesins (40) but may not express the specific isoform that interacts with Hook1 or 3. Alternatively, productive interactions with kinesin may require a specific regulatory environment not fully reconstituted in our optogenetic recruitment assays. Based on current data, we propose that mammalian Hook proteins are unidirectional, dynein-specific adaptors.

Our observations that both Hook1 and Hook3 robustly activate dynein-dependent motility led us to examine the mechanism underlying this process. We found that Hook proteins interact with dynein-dynactin, as the dynein-dynactin-Hook1 complex was efficiently precipitated by antibodies to dynactin. Furthermore, overexpression of Hook1 enhanced the dynein-dynactin interaction. In contrast to the robust co-precipitation of Hook1 with dynein and dynactin we observed with an anti-dynactin antibody, we found that the co-precipitation of the complex was disrupted when a dynein intermediate chain antibody was used. This anti-DIC antibody is known to sterically block the binding of dynein to dynactin (5). Thus, one interpretation of our observation is that Hook proteins interact directly with subunits of the dynactin complex. Another possibility is that Hook proteins effectively bind to an assembled dynein-dynactin complex. Alternatively, the DIC antibody might block the region of dynein that is necessary for Hook interaction. Interestingly, BICD2 was immunoprecipitated with the DIC antibody in other studies (30), suggesting the Hook proteins might have more extensive interactions with dynein, contacts not observed for the dynein-dynactin-BICD2 complex (7, 8). Further structural work is needed to determine the specific interaction sites within the dynein-dynactin-Hook complex.

In our induced recruitment assay and TIRF motility assay, we found that Hook proteins enhance dynein-mediated motility, increasing both velocities and run lengths. Structural studies have suggested several ways in which adaptors might modulate dynein to make it more processive. Given the apparent flexibility of the two dynein heads within the dimeric motor complex, it has been suggested that binding of dynactin locks the dynein motor heads into a more favorable conformation for motility (7). In the absence of other factors, the two heads of the dynein dimer on EM grids display a variety of distances from each other, but, in the dynein-dynactin-BICD2 complex, the motor heads are locked into a more rigid orientation, potentially allowing for more efficient stepping of the heads along the microtubule (7). As Hook proteins enhance the dynein-dynactin interaction (Fig. 3), the binding of either Hook1 or Hook3 might induce this confined dynein conformation and thus enhance processivity. Furthermore, it has been suggested that the C-terminal tail of the dynein motor causes autoinhibition of the motor (41, 42); the binding of Hook proteins to the motor complex might relieve this autoinhibition.

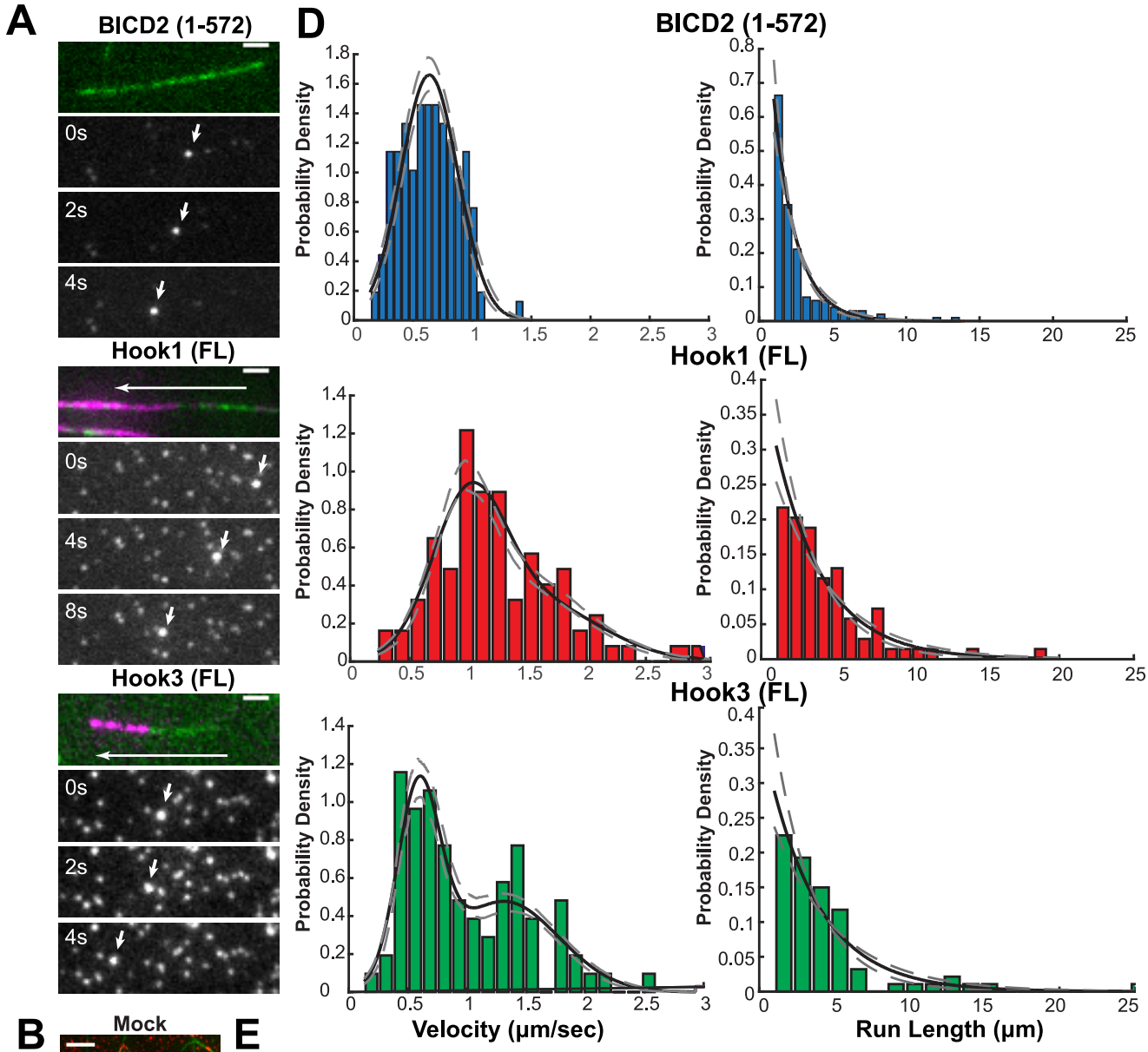

E

	Gaussian fits of Velocity				Single Exp. fits of Run Lengths
Construct	μ_1(μm/sec)	σ_1(μm/sec)	μ_2(μm/sec)	σ_2(μm/sec)	K_1
BICD2 (1-572)	0.637	0.240			0.653
Hook1 (FL)	0.999	0.305	1.555	0.552	0.306
Hook3 (FL)	0.588	0.179	1.311	0.464	0.288

FIGURE 7. **Hook proteins display high velocities and long run lengths.** *A*, example time series of particles moving to the minus end of microtubules (polarity is marked for Hk1 and Hk3; plus end shown in *green*). *Scale bars* = 2 μm. *FL*, full-length. *B*, maximum projections of Halo-Hook1 (full-length) expressed in cells under mock or dynein heavy chain (*DHC*) siRNA conditions and imaged in the TIRF assay. *Scale bars* = 5 μm. *C*, Western blot of mock and dynein heavy chain siRNA knockdown lysates used for TIRF assays. *D*, track displacement and velocity distributions for particles tracked with the ImageJ plugin TrackMate. Data were fitted with a custom maximum likelihood estimation program (38) and plotted as probability density functions with 95% confidence interval bootstrapping. (BICD2, $n = 242$; Hk1, $n = 90$; Hk3, $n = 84$). *E*, table of motility parameters based on fits from data in *D*. *F*, percent of events with a mean velocity of more than 1 μm/s. *G*, per-track standard deviation of instantaneous velocity. Data are plotted as a box plot with Tukey whiskers.

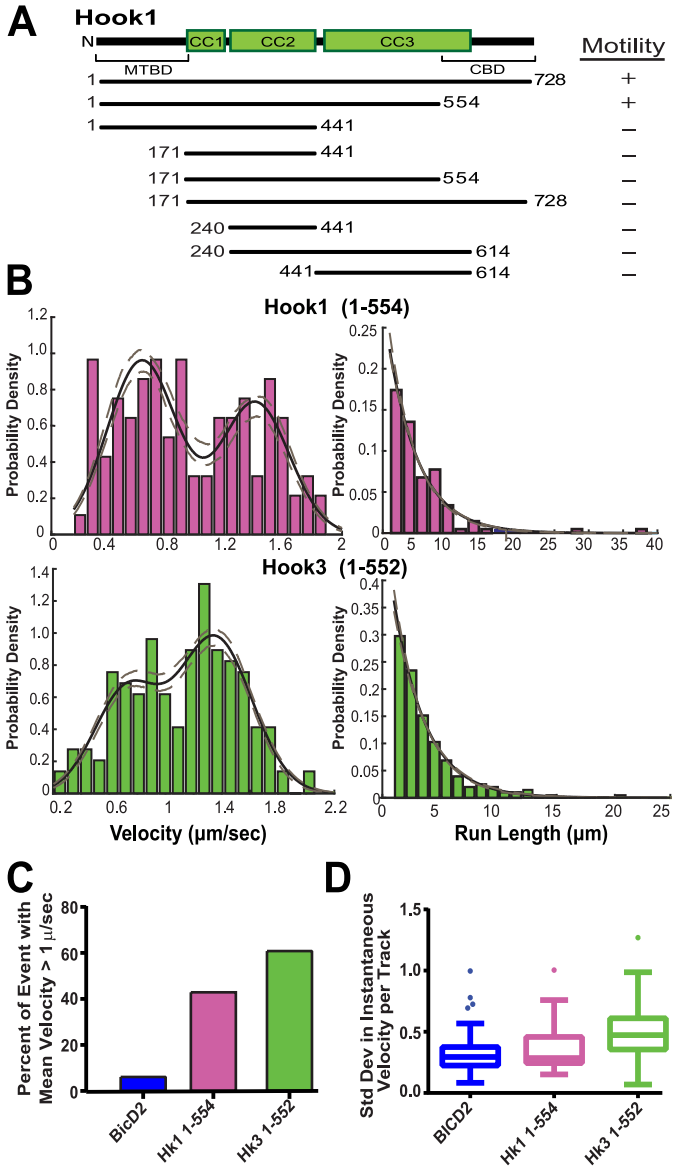

FIGURE 8. **C-terminally truncated Hook proteins display similar motility as full-length proteins.** *A*, conserved domains and predicted coiled-coil regions in Hook1 and truncated constructs below with their corresponding motility in TIRF assays (+, motility; −, no observable motility). *MTBD*, putative microtubule binding domain; *CBD*, cargo binding domain. *B*, track displacement and velocity distributions for particles tracked with the ImageJ plugin TrackMate. Data were fitted with a custom maximum likelihood estimation program (38) and plotted as probability density functions with 95% confidence interval bootstrapping (Hk1 (1–554 aa), $n = 107$; Hk3 (1–552 aa), $n = 156$. *C*, percent of events with a mean velocity of more than 1 μm/s. *D*, per-track standard deviation of instantaneous velocity. Data are plotted as a box plot with Tukey whiskers. BICD2 data are repeated from Fig. 7 for comparison.

In our TIRF assay, Hook proteins displayed higher velocities and run lengths, even compared with the previously characterized activator BICD2. Within the BICD family, there are also differences in effects on dynein-mediated velocity. For example, BICD-related protein 1 (BICDR-1) was shown to increase the velocity of Rab6 vesicles almost 2-fold more than BICD2 (17). Additionally, BICD-related proteins have an N-terminal region before the start of the coiled-coil region that is not seen in other BICD proteins. It is possible that this extra N-terminal region plays a role in enhancing velocity analogous to the enhanced motility observed in our analysis of Hook proteins, which we postulate may be due to additional contacts with dynein or dynactin mediated by the N-terminal domain. However, sequence comparisons of the N-terminal domains of Hook1 and 3 with those of BICDR-1 do not reveal significant homology, so the specific mechanisms involved may not be analogous.

Our studies with purified proteins from recombinant constructs of Hook1 and Hook3 indicate that the previously described microtubule binding domain of these Hook proteins does not directly interact with microtubules despite relatively high secondary structure conservation with other calponin homology domain proteins, such as EB1 and EB3. Calponin homology domains are typically found in actin-binding proteins and signaling proteins but have also been found in microtubule binding proteins. Our results indicate that the N-terminal calponin homology domain of Hook proteins is important for interactions with the dynein-dynactin complex and not with microtubules. Because the dynactin filament contains actin-related proteins and one β-actin subunit (8), it is possible that the calponin homology domain of Hook interacts with one or more of these dynactin subunits. Alternatively, several studies have reported specialized roles for individual dynactin subunits in tailoring specific cargo transport and could be potential interaction sites for the N-terminal region of Hook proteins. The pointed end of dynactin p25/p27 has been shown to be vital for proper endosomal transport by dynein (2, 13, 14). Because fungal Hook proteins have been linked to endosomal transport, it is possible that the N terminus of Hook proteins interacts with p25/p27, but this would require for the coiled coil of Hook proteins to be oriented in a manner opposite to that of BICD2 along the dynactin filament. If, as it is more likely, the orientation of Hook proteins is the same as that of BICD2, then the N-terminal calponin homology domain would be positioned near CapZ$\alpha\beta$ at the barbed end of the dynactin filament or in close proximity to the flexible subunit of the shoulder, p150^{Glued}. An interaction with p150^{Glued} could suggest a mechanism for induction of processive motility induced by the binding of Hook because previous work has suggested that p150^{Glued} can act as a brake for dynein via the ATP-insensitive binding of the CAP-Gly domain to the microtubule (10). It is possible that the Hook interaction with p150^{Glued} could "release" this brake to allow long processive dynein runs.

Although BICD2 is known to be tightly regulated by autoinhibition, we did not find evidence for autoinhibition of Hook proteins. Full-length constructs of either Hook1 or Hook3 were more effective than C-terminally deleted constructs in induced recruitment assays (data not shown), which is not the case for BICD2. It was reported that, in an analogous dimerization assay, full-length BICD2 had a very mild effect on organelle redistribution compared with the C-terminally truncated BICD2 construct (43), which is why most studies use a truncated, constitutively active construct. In our TIRF assay, we did not observe any motility with full-length BICD2 whereas we did with full-length Hook proteins. Thus, Hook proteins may be regulated by additional factors in the cell instead of by autoregulation.

The more divergent C-terminal regions of Hook proteins likely provide specificity for binding to particular cargoes to

regulate the utility of Hook adaptors in transport. FTS and FHIP have been suggested to link Hook proteins to early endosomes in *A. nidulans*, whereas, in mammalian systems, FTS and FHIP are suggested to link Hook proteins to the homotypic vesicular protein sorting complex for endosomal clustering (22, 25). However, FTS and FHIP seem to bind promiscuously to all three mammalian Hook homologs. Other studies on Hook proteins have identified some potential candidates for specific interactions. One study found that Hook1 can specifically interact with clathrin-independent endocytosis cargo proteins for recycling tubules from early endosomes but not other clathrin-independent endocytosis cargo proteins (24). Hook3 has been linked to scavenger receptor A to participate in the endocytotic turnover of the receptor (44), whereas Hook2 has been suggested to interact with centriolin/CEP110 to maintain centrosomal structure (23). These unique protein interactions through the C terminus of Hook proteins might provide enough specificity to regulate these adaptors to modulate motors for particular functions.

Overall, our study provides evidence that mammalian Hook proteins act as dynein adaptors to modulate dynein-mediated cargo transport. It remains to be determined how Hook proteins play a role in intracellular trafficking in more specialized cells like neurons. A recent study linked Hook proteins to Alzheimer disease, showing decreased levels of Hook proteins in diseased brains, and localized these proteins to the pathological hallmarks of Alzheimer disease, tau aggregates and amyloid plaques (45). Future work is needed to better understand the role of these adaptors in intracellular trafficking under both normal conditions and in disease states like Alzheimer disease.

Experimental Procedures

Reagents—Halo-Hook constructs were generated from the human Hook1 sequence (Uniprot code Q9UJC3) and human Hook3 sequence (Uniprot code Q86VS8) using the HaloTag from the pHTN Halo tag CMV-neo vector (Promega). An HA-Hook1 construct in the pCMV-HA vector was also generated. Full-length mouse BICD2 in the pEGFP vector (GenBank accession no. AJ250106) was a gift from A. Akhmanova and was used to generate a truncated construct spanning residues 1–572 fused to the HaloTag and cloned into pcDNA3.1. For recruitment assays, a PEX3-GFP-Halo construct was generated, including the N-terminal 42 amino acids of the human PEX3 gene for peroxisome targeting (46). BICD2-mCherry-eDHFR includes residues 1–572 of mouse BICD2, K560-mCherry-eDHFR includes residues 1–560 of human kinesin-1 heavy chain, and p150-mCherry-eDHFR includes full-length human $p150^{Glued}$ (DCTN1 sequence, GenBank accession number NM_004082). Hook-mCherry-eDHFR constructs were either full-length or truncated human constructs (Hook1 1–554 aa and Hook3 1–552 aa) as noted.

Primary antibodies used for Western blots included the following: $p150^{Glued}$ (610474, 1:5000) from BD Transduction Laboratories, DIC (MAB1618, 1:1000) from Millipore, dynein heavy chain (R-325, 1:250) from Santa Cruz Biotechnology, HaloTag (G928A, 1:1000) from Promega, Hook1 (EPR10103(B), 1:500) from Abcam, and HA (16B12, 1:1000) from Covance. For immunofluorescence staining, γ-tubulin antibody (GTU-88, 1:1000) from Sigma and secondary Alexa Fluor 633-conjugated antibody from Thermo Fisher (A21052, 1:200) were used. All HRP-conjugated secondary antibodies were from Jackson ImmunoResearch Laboratories (immunoblot 1:5000).

For brain lysates, mice (*Mus musculus*) that were wild-type and homozygous knockin DIC-eGFP-3×-FLAG were used. All animal protocols were approved by the Institutional Animal Care and Use Committee at the University of Pennsylvania. Both male and female mice (4–10 months old) were used.

For RNA interference knockdown of dynein, siRNA duplex from Dharmacon against human dynein heavy chain (GenBank accession no. NM_001376, 5′-GAGAGGAGGUUAUGUUUAAUU-3′) was used at 50 nM.

Cell Culture and Transfections—COS7 cells and HeLa cells were cultured in DMEM with 2 mM glutaMAX and 10% fetal bovine serum. Cell were transiently transfected using FuGENE 6 (Roche), and cells were harvested 18–20 h post-transfection. For RNAi transfection in knockdown experiments, Lipofectamine RNAiMax (Invitrogen) was used for transfection of siRNA duplexes, with 40- 48-h transfection for optimal knockdown.

Immunoprecipitation and Pulldown Assays—For immunoprecipitation experiments, protein G Dynabeads (Promega) were incubated with specific antibody for 10 min prior to the addition of lysates and then incubated with lysates for 15 min at room temperature. For endogenous dynein-dynactin IPs, mouse brains were homogenized in PHEM buffer (50 mM PIPES, 50 mM HEPES, 1 mM EGTA, and 2 mM $MgSO_4$) with 0.5% Triton X-100 and protease inhibitors (1 mM PMSF, 0.01 mg/ml *p*-tosyl-L-arginine methyl ester, 0.01 mg/ml leupeptin, and 0.001 mg/ml pepstatin A) and then clarified at 38,400 × *g* at 4 °C for 15 min. For $p150^{Glued}$ IP, COS7 cells expressing Hook or BICD2 constructs were lysed in 30 mM HEPES, 50 mM NaCl, 1 mM EGTA, and 2 mM $MgSO_4$ (pH 7.4) with 1 mM DTT, 0.5% Triton X-100, and protease inhibitors. Cell lysates were clarified with a 17,000 × *g* centrifugation before use.

For pulldown assays, HaloLink resin (Promega) was prepped by three washes with lysis buffer. Then lysates with Halo-tagged proteins were incubated with resin for 1 h at 4 °C to attach protein to the resins, followed by a second 1-h incubation with mouse brain lysates at 4 °C. COS7 cells expressing Halo-Hook constructs and mouse brains were both lysed in PHEM buffer and prepped as described above for IP experiments. Blots were visualized using enhanced chemiluminescence (SuperSignal West Pico chemiluminescent substrate, Thermo Scientific) with the G:Box and GeneSys digital imaging system (Syngene). Densitometry was performed with Fiji (National Institutes of Health).

Microtubule Pelleting Assays—Unlabeled tubulin was polymerized at 5 mg/ml in BRB80 (80 mM PIPES, 1 mM EGTA, and 1 mM $MgCl_2$ (pH 6.8)) with either 1 mM GTP stabilized with 20 μM Taxol or just 1 mM GMPCPP. Increasing concentrations of microtubules were incubated at 37 °C for 20 min with an equal concentration of purified protein or cell lysate. Then samples were centrifuged at 38,400 × *g* at 25 °C for 20 min. The supernatant and the pellet were then separated, denatured, and analyzed by SDS-PAGE. For cell lysate experiments, COS7 cells

transfected with HA-Hook1 (for 18–20 h) were lysed in BRB80 buffer with 0.5% Triton X-100 and protease inhibitors (as described above) and clarified with two centrifugation steps (at 17,000 and 32,000 × *g*).

For purified protein experiments, human Hook1 (Uniprot code Q9UJC3) and Hook3 (Uniprot code Q86VS8) were obtained from Open Biosystems. Hook1 fragment 1–443 was amplified by PCR, and the N-terminal tobacco etch virus protease cleavage site was added with a forward primer. Hook1 was cloned between Not1 and Sal1 sites of a modified vector, pMAL-c2x (New England Biolabs), in which a hexahistidine affinity purification tag was added N-terminally to maltose binding protein and a Sac1 site after maltose binding protein residue Asn-367 was replaced with a NotI site. Hook3 fragment 1–230 was fused in-register to 28 aa of GCN4 (MKQLEDKVEELLSKNYHLENE-VARLKKL) by overlapping primers, and the fusion construct was cloned as above. The proteins were expressed in BL21(DE3) cells (Invitrogen), grown in Terrific Broth medium at 37 °C until the A_{600} reached a value of 1.8–2.0. Expression was induced with addition of 0.5 mM isopropyl 1-thio-β-D-galactopyranoside and carried out for 16 h at 18 °C. Cells were harvested by centrifugation, resuspended in 50 mM Tris-HCl (pH 8.0), 500 mM NaCl, 5 mM imidazole, and 1 mM phenylmethylsulfonyl fluoride and lysed using a microfluidizer (Microfluidics, Westwood, MA). The proteins were first purified through a nickel-nitrilotriacetic acid affinity column (Qiagen) using a standard protocol, followed by size exclusion purification on a Superdex 200 HL 26/600 gel filtration column (GE Healthcare) in 20 mM HEPES (pH 7.5), 200 mM NaCl, 1 mM EDTA, and 1 mM DTT. Maltose binding protein was cleaved with tobacco etch virus protease and removed by additional size exclusion purification on the same column.

Inducible Recruitment Assay—HeLa cells were transiently cotransfected with PEX3-GFP-Halo and an adaptor/motor construct (BICD2-, K560-, Hook1-, Hook3-, and $p150^{Glued}$-mCherry-eDHFR) for 18–22 h. For live cell experiments, cells were plated on glass-bottom plates (World Precision Instruments), and the caged dimerizer cTMP-Halo was added 30 min prior to imaging. The dimerizer cTMP-Htag was dissolved in DMSO at 10 mM and stored in amber plastic microcentrifuge tubes at −80 °C. The dimerizer was diluted in medium to a final working concentration of 10 μM. Imaging medium was composed of phenol red-free DMEM with 25 mM HEPES (Gibco), 10% FBS, and 2 mM GlutaMAX. Live cell imaging was performed on a spinning disk confocal microscope (UltraVIEW VoX, PerkinElmer Life Sciences) with a 405-nm Ultraview Photokinesis (PerkinElmer Life Sciences) unit on an inverted microscope (Eclipse Ti, Nikon) using an Apochromat ×100, 1.49 numerical aperture oil immersion objective (Nikon) in an environmental chamber at 37 °C. Images were acquired at one frame every 2 s using a C9100–50 EMCCD camera (Hamamatsu) controlled by Volocity software (PerkinElmer Life Sciences). For whole cell photoactivation, the Photokinesis module was set at 20% laser power for 20 cycles.

For fixed recruitment assays, uncaged TMP-Htag dimerizer was added for 45 min to HeLa cells 18–20 h post-transfection. Cells were fixed with ice-cold methanol with 1 mM EGTA. Fixed cells were then stained for γ-tubulin with primary and secondary antibodies and mounted on glass coverslips with ProLong Gold anti-fade reagent (Invitrogen). Images were taken with a spinning disk UltraVIEW VoX confocal microscope with a ×100 objective (as described above), and z stacks were taken to encompass the whole depth of each cell.

Single-molecule Motility Assay—Motility assays were performed in flow chambers, each made of a glass slide and a silanized (PlusOne Repel Silane, GE Healthcare) coverslip, held together by double-sided adhesive tape and forming 15-μl volume chambers with vacuum grease. Each of the following solutions was incubated for 5 min before washout. First, a 1:40 dilution of monoclonal anti-β-tubulin antibody (T5201, Sigma) was incubated, followed by two incubations with 5% pluronic F-127 (Sigma) for blocking the coverslips. Labeled (labeling ratio of 1:40, HiLyte 488 or 647, Cytoskeleton) Taxol-stabilized microtubules were then flowed into the chamber and immobilized on β-tubulin antibodies. Finally, diluted cell lysates were flowed in with assay buffer containing 10 mM magnesium ATP, 0.3 mg/ml bovine serum albumin, 0.3 mg/ml casein, 10 mM DTT, and an oxygen-scavenging system.

For cell lysate prep, HeLa cells 18–20 h post-transfection were incubated with the Halo ligand TMR (Promega) using the guidelines of the manufacturer. Cells were lysed in 40 mM HEPES, 1 mM EDTA, 120 mM NaCl, 0.1% Triton X-100, and 1 mM magnesium ATP (pH 7.4) supplemented with protease inhibitors (as described above). Lysates were clarified with a 17,000 × *g* centrifugation. Before adding to the imaging chamber, the cell lysate extract was diluted in P12 (12 mM PIPES, 1 mM EGTA, 2 mM $MgCl_2$, and 20 μM Taxol (pH 6.8)). Cells were lysed in 100 μl of lysis buffer per 70–80% confluent 10-cm plates and then diluted 1:200 for labeled lysate with non-transfected lysate for a total of 1:50 lysate dilution for imaging. All movies were acquired at room temperature at 4 frames/s using the Nikon TIRF system (PerkinElmer Life Sciences) on an inverted Ti microscope with a ×100 objective and an ImageEM C9100–13 camera (Hamamatsu Photonics) controlled by Volocity software.

Image Analysis—For TIRF assays, particle tracking was performed using the TrackMate plugin in Fiji (37). Particle runs were tracked when the start and end of the run were seen over the course of the movie. Particles on microtubule bundles were excluded from analysis. Only processive segments of runs were used for velocity and run length measurements. A custom maximum estimation likelihood Matlab program (38) was used to fit velocity and run length data with probability density function fits. For the fixed recruitment assay, CellProfiler was used to measure the distance of peroxisomes to the microtubule organization center (47). In this program, the MTOC was manually identified, whereas both peroxisomes and the cell outline were identified by the program. Measured distances of peroxisomes from the MTOC were normalized by dividing by the longest diameter of the cell and multiplying by 100. Normalized distances were plotted as an averaged distribution, with error bars representing standard error.

Author Contributions—M. A. O., R. D., and E. L. F. H. designed the experiments. M. A. O. performed the experiments. M. T., M. B., and R. D. provided new tools and reagents. M. A. O. and E. L. F. H. wrote the manuscript. All authors reviewed the results and approved the final version of the manuscript.

Acknowledgments—We thank Karen Wallace for technical assistance; Michael Woody and Jeffery Nirschl for assistance with custom image analysis programs; Chanat Aonbangkhen for the dimerizer reagent; and Swathi Ayloo, Amy Ghiretti, and Sandra Maday for insights and discussions.

References

1. Maday, S., Twelvetrees, A. E., Moughamian, A. J., and Holzbaur, E. L. (2014) Axonal transport: cargo-specific mechanisms of motility and regulation. *Neuron* **84,** 292–309
2. Xiang, X., Qiu, R., Yao, X., Arst, H. N., Jr., Peñalva, M. A., and Zhang, J. (2015) Cytoplasmic Dynein and Early Endosome Transport. *Cell Mol. Life Sci.* **72,** 3267–3280
3. van Niekerk, E. A., Willis, D. E., Chang, J. H., Reumann, K., Heise, T., and Twiss, J. L. (2007) Sumoylation in axons triggers retrograde transport of the RNA-binding protein La. *Proc. Natl. Acad. Sci. U.S.A.* **104,** 12913–12918
4. van Spronsen, M., Mikhaylova, M., Lipka, J., Schlager, M. A., van den Heuvel, D. J., Kuijpers, M., Wulf, P. S., Keijzer, N., Demmers, J., Kapitein, L. C., Jaarsma, D., Gerritsen, H. C., Akhmanova, A., and Hoogenraad, C. C. (2013) TRAK/Milton motor-adaptor proteins steer mitochondrial trafficking to axons and dendrites. *Neuron* **77,** 485–502
5. Karki, S., and Holzbaur, E. L. (1995) affinity chromatography demonstrates a direct binding between cytoplasmic dynein and the dynactin complex. *J. Biol. Chem.* **270,** 28806–28811
6. Vaughan, K. T., and Vallee, R. B. (1995) Cytoplasmic dynein binds dynactin through a direct interaction between the intermediate chains and p150Glued. *J. Cell Biol.* **131,** 1507–1516
7. Chowdhury, S., Ketcham, S. A., Schroer, T. A., and Lander, G. C. (2015) Structural organization of the dynein-dynactin complex bound to microtubules. *Nat. Struct. Mol. Biol.* **22,** 345–347
8. Urnavicius, L., Zhang, K., Diamant, A. G., Motz, C., Schlager, M. A., Yu, M., Patel, N. A., Robinson, C. V., and Carter, A. P. (2015) The structure of the dynactin complex and its interaction with dynein. *Science* **347,** 1441–1446
9. Moughamian, A. J., and Holzbaur, E. L. (2012) Dynactin is required for transport initiation from the distal axon. *Neuron* **74,** 331–343
10. Ayloo, S., Lazarus, J. E., Dodda, A., Tokito, M., Ostap, E. M., and Holzbaur, E. L. (2014) Dynactin functions as both a dynamic tether and brake during dynein-driven motility. *Nat. Commun.* **5,** 4807
11. Holleran, E. A., Ligon, L. A., Tokito, M., Stankewich, M. C., Morrow, J. S., and Holzbaur, E. L. (2001) βIII spectrin binds to the Arp1 subunit of dynactin. *J. Biol. Chem.* **276,** 36598–36605
12. Muresan, V., Stankewich, M. C., Steffen, W., Morrow, J. S., Holzbaur, E. L., and Schnapp, B. J. (2001) Dynactin-dependent, dynein-driven vesicle transport in the absence of membrane proteins: a role for spectrin and acidic phospholipids. *Mol. Cell* **7,** 173–183
13. Zhang, J., Yao, X., Fischer, L., Abenza, J. F., Peñalva, M. A., and Xiang, X. (2011) The p25 subunit of the dynactin complex is required for dynein: early endosome interaction. *J. Cell Biol.* **193,** 1245–1255
14. Yeh, T.-Y., Quintyne, N. J., Scipioni, B. R., Eckley, D. M., and Schroer, T. A. (2012) Dynactin's pointed-end complex is a cargo-targeting module. *Mol. Biol. Cell* **23,** 3827–3837
15. Toropova, K., Zou, S., Roberts, A. J., Redwine, W. B., Goodman, B. S., Reck-Peterson, S. L., and Leschziner, A. E. (2014) Lis1 regulates dynein by sterically blocking its mechanochemical cycle. *eLife* 10.7554/eLife.03372
16. McKenney, R. J., Huynh, W., Tanenbaum, M. E., Bhabha, G., and Vale, R. D. (2014) Activation of cytoplasmic dynein motility by dynactin-cargo adapter complexes. *Science* **345,** 337–341
17. Schlager, M. A., Serra-Marques, A., Grigoriev, I., Gumy, L. F., Esteves da Silva, M., Wulf, P. S., Akhmanova, A., and Hoogenraad, C. C. (2014) Bicaudal d family adaptor proteins control the velocity of Dynein-based movements. *Cell Rep.* **8,** 1248–1256
18. Fu, M. M., and Holzbaur, E. L. (2013) JIP1 regulates the directionality of APP axonal transport by coordinating kinesin and dynein motors. *J. Cell Biol.* **202,** 495–508
19. Walenta, J. H., Didier, A. J., Liu, X., and Krämer, H. (2001) The Golgi-associated hook3 protein is a member of a novel family of microtubule-binding proteins. *J. Cell Biol.* **152,** 923–934
20. Zhang, J., Qiu, R., Arst, H. N., Jr., Peñalva, M. A., and Xiang, X. (2014) HookA is a novel dynein-early endosome linker critical for cargo movement *in vivo*. *J. Cell Biol.* **204,** 1009–1026
21. Bielska, E., Schuster, M., Roger, Y., Berepiki, A., Soanes, D. M., Talbot, N. J., and Steinberg, G. (2014) Hook is an adapter that coordinates kinesin-3 and dynein cargo attachment on early endosomes. *J. Cell Biol.* **204,** 989–1007
22. Yao, X., Wang, X., and Xiang, X. (2014) FHIP and FTS proteins are critical for dynein-mediated transport of early endosomes in *Aspergillus*. *Mol. Biol. Cell* **25,** 2181–2189
23. Szebenyi, G., Hall, B., Yu, R., Hashim, A. I., and Krämer, H. (2007) Hook2 localizes to the centrosome, binds directly to centriolin/CEP110 and contributes to centrosomal function. *Traffic* **8,** 32–46
24. Maldonado-Báez, L., Cole, N. B., Krämer, H., and Donaldson, J. G. (2013) Microtubule-dependent endosomal sorting of clathrin-independent cargo by Hook1. *J. Cell Biol.* **201,** 233–247
25. Xu, L., Sowa, M. E., Chen, J., Li, X., Gygi, S. P., and Harper, J. W. (2008) An FTS/Hook/p107(FHIP) complex interacts with and promotes endosomal clustering by the homotypic vacuolar protein sorting complex. *Mol. Biol. Cell* **19,** 5059–5071
26. Luiro, K., Yliannala, K., Ahtiainen, L., Maunu, H., Järvelä, I., Kyttälä, A., and Jalanko, A. (2004) Interconnections of CLN3, Hook1 and Rab proteins link Batten disease to defects in the endocytic pathway. *Hum. Mol. Genet.* **13,** 3017–3027
27. Ballister, E. R., Ayloo, S., Chenoweth, D. M., Lampson, M. A., and Holzbaur, E. L. (2015) Optogenetic control of organelle transport using a photocaged chemical inducer of dimerization. *Curr. Biol.* **25,** R407–R408
28. Smith, J. J., and Aitchison, J. D. (2013) Peroxisomes take shape. *Nat. Rev. Mol. Cell Biol.* **14,** 803–817
29. Hoogenraad, C. C., Akhmanova, A., Howell, S. A., Dortland, B. R., De Zeeuw, C. I., Willemsen, R., Visser, P., Grosveld, F., and Galjart, N. (2001) Mammalian Golgi-associated Bicaudal-D2 functions in the dynein-dynactin pathway by interacting with these complexes. *EMBO J.* **20,** 4041–4054
30. Splinter, D., Razafsky, D. S., Schlager, M. A., Serra-Marques, A., Grigoriev, I., Demmers, J., Keijzer, N., Jiang, K., Poser, I., Hyman, A. A., Hoogenraad, C. C., King, S. J., and Akhmanova, A. (2012) BICD2, dynactin, and LIS1 cooperate in regulating dynein recruitment to cellular structures. *Mol. Biol. Cell* **23,** 4226–4241
31. Yajima, H., Ogura, T., Nitta, R., Okada, Y., Sato, C., and Hirokawa, N. (2012) Conformational changes in tubulin in GMPCPP and GDP-Taxol microtubules observed by cryoelectron microscopy. *J. Cell Biol.* **198,** 315–322
32. Alushin, G. M., Lander, G. C., Kellogg, E. H., Zhang, R., Baker, D., and Nogales, E. (2014) High-resolution microtubule structures reveal the structural transitions in $\alpha\beta$-tubulin upon GTP hydrolysis. *Cell* **157,** 1117–1129
33. Waterman-Storer, C. M., Karki, S., and Holzbaur, E. L. (1995) The p150Glued component of the dynactin complex binds to both microtubules and the actin-related protein centractin (Arp-1). *Proc. Natl. Acad. Sci. U.S.A.* **92,** 1634–1638
34. Zhang, R., Alushin, G. M., Brown, A., and Nogales, E. (2015) Mechanistic origin of microtubule dynamic instability and its modulation by EB proteins. *Cell* **162,** 849–859
35. Slep, K. C., and Vale, R. D. (2007) Structural basis of microtubule plus end tracking by XMAP215, CLIP-170, and EB1. *Mol. Cell* **27,** 976–991
36. Malone, C. J., Misner, L., Le Bot, N., Tsai, M.-C., Campbell, J. M., Ahringer, J., and White, J. G. (2003) The *C. elegans* hook protein, ZYG-12, mediates

the essential attachment between the centrosome and nucleus. *Cell* **115,** 825–836
37. Schindelin, J., Arganda-Carreras, I., Frise, E., Kaynig, V., Longair, M., Pietzsch, T., Preibisch, S., Rueden, C., Saalfeld, S., Schmid, B., Tinevez, J.-Y., White, D. J., Hartenstein, V., Eliceiri, K., Tomancak, P., and Cardona, A. (2012) Fiji: an open-source platform for biological-image analysis. *Nat. Methods* **9,** 676–682
38. Woody, M. S., Lewis, J. H., Greenberg, M. J., Goldman, Y. E., and Ostap, E. M. (2016) MEMLET: An easy-to-use tool for data fitting and model comparison using maximum likelihood estimation. *Biophys. J.*, in press
39. Terawaki, S., Yoshikane, A., Higuchi, Y., and Wakamatsu, K. (2015) Structural basis for cargo binding and autoinhibition of Bicaudal-D1 by a parallel coiled-coil with homotypic registry. *Biochem. Biophys. Res. Commun.* **460,** 451–456
40. Maliga, Z., Junqueira, M., Toyoda, Y., Ettinger, A., Mora-Bermúdez, F., Klemm, R. W., Vasilj, A., Guhr, E., Ibarlucea-Benitez, I., Poser, I., Bonifacio, E., Huttner, W. B., Shevchenko, A., and Hyman, A. A. (2013) A genomic toolkit to investigate kinesin and myosin motor function in cells. *Nat. Cell Biol.* **15,** 325–334
41. Torisawa, T., Ichikawa, M., Furuta, A., Saito, K., Oiwa, K., Kojima, H., Toyoshima, Y. Y., and Furuta, K. (2014) Autoinhibition and cooperative activation mechanisms of cytoplasmic dynein. *Nat. Cell Biol.* **16,** 1118–1124
42. Nicholas, M. P., Höök, P., Brenner, S., Wynne, C. L., Vallee, R. B., and Gennerich, A. (2015) Control of cytoplasmic dynein force production and processivity by its C-terminal domain. *Nat. Commun.* **6,** 6206
43. Hoogenraad, C. C., Wulf, P., Schiefermeier, N., Stepanova, T., Galjart, N., Small, J. V., Grosveld, F., de Zeeuw, C. I., and Akhmanova, A. (2003) Bicaudal D induces selective dynein-mediated microtubule minus end-directed transport. *EMBO J.* **22,** 6004–6015
44. Sano, H., Ishino, M., Krämer, H., Shimizu, T., Mitsuzawa, H., Nishitani, C., and Kuroki, Y. (2007) The microtubule-binding protein Hook3 interacts with a cytoplasmic domain of scavenger receptor A. *J. Biol. Chem.* **282,** 7973–7981
45. Herrmann, L., Wiegmann, C., Arsalan-Werner, A., Hilbrich, I., Jäger, C., Flach, K., Suttkus, A., Lachmann, I., Arendt, T., and Holzer, M. (2015) Hook proteins: association with Alzheimer pathology and regulatory role of hook3 in amyloid β generation. *PLoS ONE* **10,** e0119423
46. Kapitein, L. C., Schlager, M. A., van der Zwan, W. A., Wulf, P. S., Keijzer, N., and Hoogenraad, C. C. (2010) Probing intracellular motor protein activity using an inducible cargo trafficking assay. *Biophys. J.* **99,** 2143–2152
47. Carpenter, A. E., Jones, T. R., Lamprecht, M. R., Clarke, C., Kang, I. H., Friman, O., Guertin, D. A., Chang, J. H., Lindquist, R. A., Moffat, J., Golland, P., and Sabatini, D. M. (2006) CellProfiler: image analysis software for identifying and quantifying cell phenotypes. *Genome Biol.* **7,** R100
48. Ballister, E. R., Aonbangkhen, C., Mayo, A. M., Lampson, M. A., and Chenoweth, D. M. (2014) Localized light-induced protein dimerization in living cells using a photocaged dimerizer. *Nat. Commun.* **5,** 5475